

Channel diversity in random wireless networks

Kostas Stamatiou, John G. Proakis and James R. Zeidler

Abstract

The goal of this paper is to explore the benefits of channel diversity in wireless ad hoc networks. Our model is that of a Poisson point process of transmitters, each with a receiver at a given distance. A packet is divided in blocks which are transmitted over different subbands that are determined by random frequency hopping. At the receiver, a maximum-likelihood decoder is employed to estimate the transmitted packet/codeword. We find that, if L is the Hamming distance of the employed error correction code and ϵ is a constraint on the packet error probability, the transmission capacity of the network is proportional to $\epsilon^{1/L}$, when $\epsilon \rightarrow 0$. The proportionality constant depends on the geometry of the symbol constellation, the packet length and the number of receive antennas. This result implies that, at the cost of a moderate decoding complexity, large gains can be achieved by a simple interference randomization scheme during packet transmission.

We also address practical issues such as channel estimation and power control. We find that reliable channel information can be obtained at the receiver without significant rate loss and demonstrate that channel inversion power control can increase the network transmission capacity.

Index Terms

Frequency hopping, interference diversity, bit-interleaved coded modulation (BICM), Poisson point process, transmission capacity

I. INTRODUCTION

The study of random wireless networks has recently gathered a lot of attention in the research community [1]–[3]. The main theme of this work is the use of tools from stochastic geometry, in order to provide analytical performance results and develop insights for an ensemble of networks and different physical, MAC and network layer strategies. A central assumption is that the network consists of a Poisson point process of transmitters, and each transmitter (TX)

The support of the ARO MURI project on space-time processing for ad hoc networks is gratefully acknowledged.

has a corresponding receiver (RX) at a given distance. A popular metric that quantifies the network performance is the transmission capacity, defined as the maximum spatial density of transmissions, multiplied by their rate, such that a constraint on the packet error rate is satisfied [1].

In the majority of existing papers, interference from concurrent transmissions is considered as noise and an outage probability approach is taken to model packet successes: given the TX locations and the channels between the TXs and the reference RX, which are assumed to be constant during the transmission of a packet, a packet is successfully received if the signal-to-interference-ratio (SIR) is larger than a certain threshold. In information-theoretical terms, assuming the interfering TXs are transmitting symbols from a Gaussian alphabet, a packet reception occurs when the channel mutual information is at least equal to the desired information rate [4].

In this paper, as in [5], we take an alternative approach and explore the impact of channel randomization *within* the transmission of a packet. Our motivation stems from the well known fact that channel diversity can be exploited through error correction coding in order to yield performance gains. Specifically, we consider a bit-interleaved coded modulation scheme (BICM) [6], in conjunction with random frequency hopping (FH), maximal ratio combining (MRC) and maximum likelihood (ML) decoding at the RX. Coding combined with FH exploits frequency diversity, if the hopping distance is larger than the coherence bandwidth of the channel fading, and interference diversity, as the set of interfering transmitters over each dwell is potentially different. We analyze the performance of this scheme in terms of the codeword/packet error probability and evaluate the transmission capacity as a function of the code diversity order and the size of the antenna array at the RX. Since an averaging over different channel states takes place within a packet, the information rate of the typical TX-RX link is upper-bounded by the ergodic capacity for which we provide tight upper and lower bounds. We also address practical physical layer issues such as channel estimation, power control (PC) and channel correlation, and assess their effect on the performance via simulation.

A. Related work

Several papers have dealt with the performance analysis of coded FH systems under multiple-access (MA) interference, as well as partial-band interference (see, e.g., [7], [8] and ch. 12 of [9]).

A common feature of such systems is that the performance can be dramatically improved if the decoder is aware of the interference levels across the codeword. If a Reed-Solomon (RS) code is employed, the decoder declares an erasure when a symbol has been “hit”; in the case of soft-decoding, the metrics in the Viterbi decoder are weighted by the respective SIRs. In [10], RS coding combined with FSK modulation is considered in a Poisson field of interferers and the impact of the code rate on the information efficiency, i.e., the product (packet success probability) \times (transmission distance) \times (rate), is explored. More recently, [11] has extended the work in [10] to accommodate differential unitary space-time modulation and unknown fast time-varying channels.

The use of spread-spectrum (SS) communication for ad hoc networks is discussed in [12]. The authors make an argument against interference averaging which they define as “. . . using direct-sequence (DS) SS or fast FH¹ to proportionally reduce the interference level” and advocate hopping at the packet level, or interference avoidance (IA), as the preferable MA scheme for ad hoc networks. While the near-far problem of DS-SS in a decentralized environment - where PC is absent - is clear, it is not obvious why slow FH might be preferable to fast FH, apart from the fact that the former induces less overhead in terms of code acquisition and synchronization.

B. Contributions

This paper demonstrates that considerable gains in terms of network capacity are possible, by combining FH during packet transmission and error correction coding of modest complexity. If L is the Hamming distance of the convolutional code employed at the TX, λ is the density of TXs and M is the number of subbands, we show that, as $\lambda/M \rightarrow 0$, the codeword error probability follows the power law $\eta(\frac{\lambda}{M})^L$, $\eta > 0$. This implies that, for $\epsilon \rightarrow 0$, the transmission capacity is proportional to $\epsilon^{1/L}$ where ϵ is the constraint placed on the codeword error probability. The proportionality constant depends on the geometry of the symbol constellation, the codeword length, as well as the term $N^{2/b}$ where N is the number of RX antennas and $b > 2$, is the propagation exponent. We also derive upper and lower bounds on the ergodic capacity C of the typical TX-RX link; specifically, we show that $C > \frac{1}{\alpha} \log_2 (\mu N^\alpha \frac{M}{\lambda})$, where $\mu > 0$ is an appropriately defined constant.

¹Fast FH refers to hopping on the order of a symbol or a few symbols, while slow FH, or interference avoidance, refers to hopping at the packet level.

Practical physical layer issues are discussed such as channel estimation, PC and channel correlation. We demonstrate via simulation that, with an acceptable rate loss due to the transmission of pilot symbols, accurate channel state information (CSI) can be obtained for decoding. With respect to PC, it is shown that channel inversion can actually improve the performance, since the error correction code protects the RX from the deep fades of its nearby interferers. Finally, the impact of the channel correlation is assessed as the number of subbands and/or the number of dwells is decreased and it is shown that the gains compared to slow FH are still significant.

C. Paper organization and notation

The rest of the paper is organized as follows. Section II introduces our network and physical layer models in detail. In Section III we derive the statistics of the SIR and determine the performance of the decoder under perfect CSI. The transmission capacity is defined and evaluated in Section IV. Section V discusses practical physical layer considerations and Section VI presents our numerical results. Section VII concludes the paper.

A real (circularly symmetric complex) Gaussian random variable x with mean 0 and variance σ^2 is denoted as $x \sim \mathcal{N}(0, \sigma^2)$ ($x \sim \mathcal{CN}(0, \sigma^2)$). A central chi-square r.v. x with parameter $1/2$ and n degrees of freedom is denoted as $x \sim \chi_n^2$. \mathbf{I}_n is the $n \times n$ identity matrix. $(\cdot)^T$ and $(\cdot)^H$ denote the transpose and conjugate transpose operations, respectively. $[\mathbf{X}]_{n,t}$ denotes the (n, t) element of matrix \mathbf{X} . The symbol “ \simeq ” is employed to denote asymptotic equality of two functions. Finally, a list of symbols commonly used throughout the paper is provided in Table I.

II. SYSTEM MODEL

A. General

We consider a network of TXs, each with a RX at a fixed distance R and random orientation. The locations of the TXs are drawn independently according to a homogeneous Poisson point process Π of density λ . The TXs transmit packets to their corresponding RXs concurrently and in a synchronized manner. Typically, the locations of the nodes are constant for at least the duration of a packet.

The bandwidth is divided into M subbands. The channel between a typical TX-RX pair over a subband comprises flat Rayleigh fading and path loss according to the law r^{-b} , where $b > 2$ is the propagation exponent. We assume that the coherence bandwidth of the fading is equal

to the width of a subband, while the coherence time can be equal to the duration of a packet slot or the duration of a *dwell*, which will be defined shortly. We also consider an interference-limited scenario, i.e., additive noise at the RX is assumed negligible, such that interference from concurrent transmissions is the only cause for packet errors. Initially, we assume that the power transmitted from all TXs is the same and normalized to one. Issues of PC to compensate for long-term fading, e.g., shadowing, are discussed in Section V.

Assume that a packet corresponds to L_b binary information bits, b_1, \dots, b_{L_b} , which are the input to a convolutional encoder of rate $R_c < 1^2$. The bits $c_1, \dots, c_{k'}, \dots, c_{L_b/R_c}$ of the output codeword are interleaved and Gray-mapped to symbols $x_1, \dots, x_k, \dots, x_{L_b/(R_c M_c)}$ from a complex PSK or QAM constellation \mathcal{X} of size $|\mathcal{X}| = 2^{M_c}$, zero mean and unit average power. We assume that the one-to-one interleaver mapping $k' \leftrightarrow (k, j_{k'})$, where $j_{k'} = 1, \dots, M_c$ is the position of $c_{k'}$ in the symbol x_k , is known at the RX. Next in the TX chain, the symbol sequence is divided in $D = L_b/(R_c M_c T_d)$ groups³ of size T_d and each group is transmitted in a dwell, over a subband which is randomly⁴ selected with probability $1/M$. If we denote the data symbols of the d^{th} dwell, $d = 1, \dots, D$, as \mathbf{x}_d^T the sequence $\{\mathbf{x}_d^T\}_{d=1}^D$ constitutes a packet. For convenience, we assume all transmissions are synchronized at the dwell level. This is a worst-case scenario in terms of the level of the interference power over a dwell (the issue of asynchronous transmissions is discussed in Section V).

Consider a typical TX and its corresponding RX, both specified by index 0, i.e., TX₀ and RX₀. If RX₀ is equipped with an antenna array of size $N \geq 1$, the received data matrix in dwell d is⁵

$$\mathbf{Y}_{d,0} = \mathbf{h}_{d,0} \mathbf{x}_{d,0}^T + R^{b/2} \sum_{i \in \Pi} e_{d,i} r_i^{-b/2} e^{i\phi_i} \mathbf{h}_{d,i} \mathbf{x}_{d,i}^T, \quad (1)$$

where $\mathbf{h}_{d,0} \sim \mathcal{CN}(\mathbf{0}, \mathbf{I}_N)$ is the fading vector between TX₀ and RX₀; $e_{d,i}$ is the indicator of whether TX i , at distance r_i from RX₀ and denoted as TX _{i} , occupies the same subband as

²We assume that the encoder is trellis-terminated [13], i.e., it is forced to start from and end at the zero-state. This results in a small rate loss which is not taken into account.

³For convenience, we assume that the quotients $L_b/(R_c M_c)$ and $D = L_b/(R_c M_c T_d)$ are integer.

⁴In reality, the hopping pattern is determined pseudorandomly and is known at the RX. However, the model of random subband selection is convenient for analytical purposes.

⁵We assume that the average received power R^{-b} per antenna is known at RX₀. We have taken it into account in the interference portion of the received signal because it is convenient in terms of notation in the remainder of the paper.

TX₀ in dwell d , i.e., $e_{d,i} = 1$ with probability $1/M$ and $e_{d,i} = 0$ with probability $1 - 1/M$; $\mathbf{h}_{d,i} \sim \mathcal{CN}(\mathbf{0}, \mathbf{I}_N)$ is the fading vector between TX _{i} and RX₀; $\mathbf{x}_{d,i}^T$ is the group of data symbols transmitted by TX _{i} in dwell d ; and ϕ_i is a random phase, uniformly distributed in $[0, 2\pi)$, which models the phase offset between the RX₀ and TX _{i} . Note that the subscript d in the fading vectors indicates that, in general, depending on the coherence time, these may vary independently from dwell to dwell.

Let $\mathbf{W}_{d,0}$ denote the interference term in (1). Since the elements of $\mathbf{x}_{d,i}$ are independent and zero-mean, the same holds for the elements of $\mathbf{W}_{d,0}$. Moreover, given $\{r_i\}$, we assume that $[\mathbf{W}_{d,0}]_{n,t} \sim \mathcal{CN}(0, z_{d,0})^6$, $n = 1, \dots, N$, $t = 1, \dots, T_d$, and $z_{d,0} \triangleq \sum_{i \in \Pi} e_{d,i} r_i^{-b}$ is the interference power in dwell d seen by RX₀. RX₀ can obtain knowledge of $\mathbf{h}_{d,0}$ and $z_{d,0}$ with the help of pilot symbols which are transmitted at the beginning of the dwell. Presently, we assume that they are perfectly known; a straightforward channel estimation algorithm is presented in Section V.

B. Equivalent channel model and decoding

The reference RX performs MRC, i.e., it evaluates the product $\frac{\mathbf{h}_{d,0}^H}{\|\mathbf{h}_{d,0}\|^2} \mathbf{Y}_{d,0}$. From (1), we have

$$\frac{\mathbf{h}_d^H}{\|\mathbf{h}_d\|^2} \mathbf{Y}_d = \mathbf{x}_d^T + \frac{\mathbf{h}_d^H}{\|\mathbf{h}_d\|^2} \mathbf{W}_d, \quad (2)$$

where we have omitted the index 0 in order to simplify the notation. As a result, we have the following equivalent channel model for data symbol x_k , $k = (d-1)T_d + 1, \dots, dT_d$, which is transmitted in dwell d

$$y_k = x_k + w_k \quad (3)$$

where, $w_k \sim \mathcal{CN}(0, \gamma_k^{-1})$, given the equivalent SIR $\gamma_k = \frac{a_k}{z_k}$. The r.v. a_k is chi-square distributed with $2N$ degrees of freedom, i.e., $a_k \sim \chi_{2N}^2$. Moreover, due to the fact that the locations of the interferers in each dwell are a realization of a Poisson process on the plane with density λ/M , it is known that z_k is an α -stable random variable with stability exponent $\alpha = 2/b$ [14], [15]. Its moment generating function (mgf) is [14]

$$\Phi_z(s) = \mathbb{E}[e^{-zs}] = e^{-\frac{\lambda s}{M} s^\alpha}, \quad s > 0. \quad (4)$$

⁶The Gaussian assumption for the interference is exact if the elements of $x_{d,i}$ are selected from a PSK constellation and an approximation if they are selected from a QAM constellation.

where

$$\delta \triangleq \pi\Gamma(1 - \alpha)R^2. \quad (5)$$

The sequence $\{y_k, \gamma_k\}_{k=1}^{DT_d}$ is the input to the decoder which decides that the codeword \hat{c} was transmitted according to the simplified ML criterion (eq.(9), [6])

$$\hat{c} = \arg \min_{\mathbf{c}} \sum_{k'=1}^{L_b/R_c} \gamma_k \min_{x \in \mathcal{X}_{c_{k'}}^{j_{k'}}} \{|y_k - x|^2\} \quad (6)$$

where $\mathcal{X}_{c_{k'}}^{j_{k'}}$ denotes the set of constellation symbols that have bit $c_{k'}$ at position $j_{k'}$, where $j_{k'} = 1, \dots, M_c$. The weighting of each distance metric by the respective SIR reflects the confidence of the decoder in that metric.

III. ANALYSIS

This section is primarily devoted to the performance analysis of decoder (6). In order to round out the analysis, in Section III-D, we also derive upper and lower bounds to the ergodic capacity of channel (3). Since the scheme presented in Section II induces an ‘‘averaging’’ over different channel states within the packet, the ergodic capacity is an upper bound to the information rate of the typical TX-RX link.

A. Decoder performance

The codeword - or frame - error probability (FEP) of decoder (6), P_e , is upper-bounded as [13]

$$P_e \leq L_b \sum_{l=L, L+1, \dots} w_l P_l \quad (7)$$

where P_l is the probability of a length- l error event, or pairwise error probability, and w_l is the number of length- l error events. The minimum length of an error event L , i.e., the Hamming distance, as well as the weight distribution $\{w_l\}$ depend on the particular code employed.

We now assume that, due to random interleaving, the sequence of l symbols that corresponds to a sequence of l coded bits encounters *independent* SIR conditions (this assumption is discussed in Section V). From [6], [16], P_l can be upper-bounded as

$$P_l \leq \bar{P}_l = \frac{1}{\pi} \int_0^{\pi/2} \left(\frac{1}{M_c 2^{M_c}} \sum_{(x, x') \in \mathcal{X}} \Phi_\gamma \left(\frac{|x - x'|^2}{4 \sin^2 \theta} \right) \right)^l d\theta \quad (8)$$

where $\Phi_\gamma(s)$ is the mgf of the SIR γ , i.e., $\Phi_\gamma(s) = \mathbb{E}[e^{-\gamma s}]$, $s > 0$ (the time index k has been removed as it is of no consequence). (x, x') are all possible $M_c 2^{M_c}$ nearest-neighbor pairs in \mathcal{X} which have complementary bits in position j , $j = 1, \dots, M_c$ [6], e.g., for 4QAM (QPSK) constellations with Gray mapping, all such pairs are at the minimum constellation distance d_{\min} . Note that, in the limit of large $E[\gamma]$ ⁷, $\bar{P}_l \simeq P_l$ [6].

From (7), a further upper bound to P_e is

$$\bar{P}_e = L_b \sum_{l=L, L+1, \dots} w_l \bar{P}_l. \quad (9)$$

The evaluation of \bar{P}_l in (8) is possible by numerical integration, provided that $\Phi_\gamma(s)$ is known. The derivation of $\Phi_\gamma(s)$ is the topic of the following subsection.

B. Statistics of γ

The probability density function (pdf) of γ is given by the following lemma.

Lemma 1: The pdf of the SIR γ is given by

$$f_\gamma(\gamma) = \frac{1}{(N-1)!} \frac{e^{-\frac{\lambda\delta}{M}\gamma^\alpha}}{\gamma} \sum_{n=1}^N \frac{|\beta_n^N|}{n!} \left(\frac{\lambda\delta}{M} \gamma^\alpha \right)^n \quad (10)$$

where

$$\beta_n^N = \sum_{m=1}^n (-1)^m \binom{n}{m} (\alpha m)_N, \quad n = 1, \dots, N \quad (11)$$

and $(\alpha m)_N \triangleq \alpha m \dots (\alpha m - N + 1)$ is the falling sequential product.

Proof: The cumulative distribution function (cdf) of γ , $F_\gamma(\gamma)$, is by definition

$$F_\gamma(\gamma) = \mathbb{P}(a \leq \gamma z) = \int_0^{+\infty} F_a(\gamma z) f_z(z) dz \quad (12)$$

where

$$F_a(a) = 1 - e^{-a} \sum_{n=0}^{N-1} \frac{a^n}{n!} = 1 - \frac{\Gamma(N, a)}{(N-1)!} \quad (13)$$

is the cdf of the chi-square r.v. a and

$$\Gamma(\zeta, x) = \int_x^{+\infty} e^{-t} t^{\zeta-1} dt, \quad x \geq 0 \quad (14)$$

⁷In the context of this paper, this corresponds to the interferer point process in each dwell being sparse, i.e., $\lambda/M \rightarrow 0$.

is the incomplete gamma function (p.949, [17]). Substituting (13) in (12) and taking the derivative, the pdf of γ is given by

$$\begin{aligned} f_\gamma(\gamma) &= -\frac{1}{(N-1)!} \int_0^{+\infty} \frac{d\Gamma(N, \gamma z)}{d\gamma} f_z(z) dz = \frac{\gamma^{N-1}}{(N-1)!} \int_0^{+\infty} f_z(z) z^N e^{-\gamma z} dz \\ &= \frac{(-1)^N \gamma^{N-1}}{(N-1)!} \frac{d^N \Phi_z(\gamma)}{d\gamma^N} \end{aligned} \quad (15)$$

where we have used the identity (p.951, [17]) $\frac{d\Gamma(\zeta, x)}{dx} = -x^{\zeta-1} e^{-x}$ and the Laplace transform property⁸

$$f_z(z) z^N \xleftrightarrow{\mathcal{L}} (-1)^N \frac{d^N \Phi_z(s)}{ds^N}.$$

From the identity for the N^{th} derivative of a composite function (0.430.1, p.24, [17]), after some algebra, we obtain

$$\frac{d^N \Phi_z(s)}{ds^N} = s^{-N} e^{-\frac{\lambda\delta}{M}s^\alpha} \sum_{n=1}^N \frac{\beta_n^N}{n!} \left(\frac{\lambda\delta}{M} s^\alpha \right)^n \quad (16)$$

where β_n^N is given by (11). From (16) and (15) we have that

$$f_\gamma(\gamma) = \frac{1}{(N-1)!} \frac{e^{-\frac{\lambda\delta}{M}\gamma^\alpha}}{\gamma} \sum_{n=1}^N \frac{(-1)^N \beta_n^N}{n!} \left(\frac{\lambda\delta}{M} \gamma^\alpha \right)^n. \quad (17)$$

In order to derive (10) from (17), we need to show that $(-1)^N \beta_n^N \geq 0$. Once again, using the identity for the N^{th} derivative of a composite function, β_n^N can be written as the following derivative evaluated at $x = 1$.

$$\beta_n^N = \left. \frac{d^N (1 - x^\alpha)^n}{dx^N} \right|_{x=1}. \quad (18)$$

From (18), the following iterative relation can be proved for $N \geq 2$

$$\beta_n^N = \sum_{m_1=1}^N \binom{N}{m_1} \beta_1^{m_1} \beta_{n-1}^{N-m_1}. \quad (19)$$

By successive application of (19), we obtain

$$\frac{(-1)^N \beta_n^N}{N!} = \sum_{m_1=1}^N \sum_{m_2=1}^{N-m_1} \cdots \sum_{m_{n-1}=1}^{N-m_1-\cdots-m_{n-2}} (-1)^{m_1} \beta_1^{m_1} (-1)^{m_2} \beta_1^{m_2} \cdots (-1)^{m_n} \beta_1^{m_n} \quad (20)$$

where $m_n = N - m_{n-1} - \cdots - m_1$. However, $(-1)^N \beta_1^N \geq 0$, since, by (11), $(-1)^N \beta_1^N = (-1)^{N+1} \alpha(\alpha-1) \cdots (\alpha-N+1)$ and $\alpha = 2/b < 1$. Therefore, $(-1)^N \beta_n^N \geq 0$ for $n = 1, \dots, N$. ■

⁸This identity is also employed in [18], in order to derive the ccdf of γ .

As expected, increasing the spatial diversity order N increases $f_\gamma(\gamma)$, as more positive terms are added to the polynomial in (10).

By the definition of the mgf of γ and (10), we have

$$\Phi_\gamma(s) = \frac{1}{(N-1)!} \sum_{n=1}^N \frac{|\beta_n^N|}{n!} \left(\frac{\lambda\delta}{M}\right)^n \int_0^{+\infty} \gamma^{\alpha n-1} e^{-\frac{\lambda\delta}{M}\gamma^\alpha - s\gamma} d\gamma. \quad (21)$$

This integral can be evaluated numerically for any $s > 0$ using Gauss-Laguerre quadrature.

C. Approximations

The numerical evaluation of \bar{P}_l using (21) provides little insight on how the decoder performance depends on the system parameters. In this section, we examine the decoder performance when $\lambda/M \rightarrow 0$, i.e., the interferer point process in each dwell is sparse. This implies that the network is operated in a regime of small FEP, i.e., typically $\bar{P}_e \leq \epsilon$, with $\epsilon \leq 0.1$.

Let $B(\zeta_1, \zeta_2)$, $\zeta_1, \zeta_2 > 0$ denote the beta function. Our main result is stated in the following proposition.

Proposition 1: If $\lambda/M \rightarrow 0$, then $\bar{P}_l = \eta(\frac{\lambda}{M})^l + o\left(\left(\frac{\lambda}{M}\right)^l\right)$, where \bar{P}_l is defined in (8) and η is a positive constant. Moreover,

$$\bar{P}_l \simeq \frac{2^{4\alpha l-1}}{\pi} B\left(\alpha l + \frac{1}{2}, \alpha l + \frac{1}{2}\right) \left(\frac{\alpha B(N-\alpha, \alpha) \lambda \pi R^2}{d_{\mathcal{X}}^2 M}\right)^l \quad (22)$$

where

$$d_{\mathcal{X}}^2 = \left(\frac{1}{M_c 2^{M_c}} \sum_{x, x' \in \mathcal{X}} \frac{1}{|x - x'|^{2\alpha}}\right)^{-1}. \quad (23)$$

Proof: Omitting the term $e^{-\frac{\lambda\delta}{M}\gamma^\alpha}$ in (21), an upper bound to $\Phi_\gamma(s)$ for all $s > 0$ is

$$\begin{aligned} \overline{\Phi_\gamma(s)} &= \frac{1}{(N-1)!} \sum_{k=1}^N \frac{|\beta_k^N|}{k!} \left(\frac{\lambda\delta}{M}\right)^k \int_0^{+\infty} \gamma^{\alpha k-1} e^{-\gamma s} d\gamma \\ &= \frac{1}{(N-1)!} \sum_{k=1}^N \frac{|\beta_k^N|}{k!} \left(\frac{\lambda\delta}{M}\right)^k s^{-\alpha k} \Gamma(\alpha k) \\ &= \frac{\alpha B(N-\alpha, \alpha)}{\Gamma(1-\alpha)} \left(\frac{\lambda\delta}{M}\right) s^{-\alpha} + \frac{1}{(N-1)!} \sum_{k=2}^N \frac{|\beta_k^N|}{k!} \left(\frac{\lambda\delta}{M}\right)^k s^{-\alpha k} \Gamma(\alpha k). \end{aligned} \quad (24)$$

where we have used the identities $\Gamma(\zeta + 1) = \zeta \Gamma(\zeta)$ and [17]

$$B(\zeta_1, \zeta_2) = \frac{\Gamma(\zeta_1)\Gamma(\zeta_2)}{\Gamma(\zeta_1 + \zeta_2)}. \quad (25)$$

From (24) and (8), we can see that, for $\lambda/M \rightarrow 0$, $\bar{P}_l = \eta(\frac{\lambda}{M})^l + o\left((\frac{\lambda}{M})^l\right)$, with η appropriately defined.

Note that the bound in (24) is tight as $\lambda/M \rightarrow 0$. Ignoring the higher order terms, for $\lambda/M \rightarrow 0$, we thus have that

$$\Phi_\gamma(s) \simeq \overline{\Phi_\gamma(s)} \simeq \pi\alpha R^2 B(N - \alpha, \alpha) s^{-\alpha} \frac{\lambda}{M}. \quad (26)$$

Substituting (26) in (8)

$$\bar{P}_l \simeq \left(\pi\alpha R^2 B(N - \alpha, \alpha) d_{\mathcal{X}}^{-2} \frac{\lambda}{M} \right)^l \frac{4^\alpha}{\pi} \int_0^{\pi/2} (\sin \theta)^{2\alpha l} d\theta \quad (27)$$

where $d_{\mathcal{X}}^2$ is defined in (23). Employing the identity (p.412, [17])

$$\int_0^{\pi/2} (\sin \theta)^{2\alpha l} d\theta = 2^{2\alpha l - 1} B(\alpha l + 1/2, \alpha l + 1/2)$$

we obtain (22). ■

Remarks: Proposition 1 states that, for $\lambda/M \rightarrow 0$, the Hamming distance of the convolutional code determines the *diversity order*, i.e., the slope of the curve \bar{P}_e vs. λ/M . Moreover, the spatial diversity order N introduces an array or *coding gain* through the factor $B(N - \alpha, \alpha)^L$. To obtain further insight on this factor, we examine the trend of the beta function for large N . For large ζ , it holds that $\Gamma(\zeta) \sim \sqrt{2\pi} \zeta^{\zeta - 1/2} e^{-\zeta}$ ([17], p.945), therefore

$$\frac{\Gamma(N - \alpha)}{\Gamma(N)} \simeq N^{-\alpha} \left(1 - \frac{\alpha}{N}\right)^{N - \alpha - \frac{1}{2}} e^\alpha.$$

However, it is easy to verify that $\lim_{N \rightarrow \infty} \left(1 - \frac{\alpha}{N}\right)^{N - \alpha - \frac{1}{2}} = e^{-\alpha}$, so, from (25), $B(N - \alpha, \alpha) \simeq \Gamma(\alpha) N^{-\alpha}$. As a result, for large N , the coding gain is proportional to $N^{-L\alpha}$.

A final observation is that, similarly to [6], the parameter $d_{\mathcal{X}}^2$ is the harmonic mean of the minimum squared Euclidean distance between the nearest neighbor pairs defined in Section III-A, raised to the stability exponent α . Assuming unit average energy, for BPSK we have $d_{\mathcal{X}, \text{BPSK}}^2 = 2^{-2\alpha}$, while for 4QAM and 16QAM with Gray mapping, we have $d_{\mathcal{X}, 4\text{QAM}}^2 = 2^{-\alpha}$ and $d_{\mathcal{X}, 16\text{QAM}}^2 = \frac{3}{4}(\sqrt{\frac{2}{5}})^{-2\alpha} + \frac{1}{4}(2\sqrt{\frac{2}{5}})^{-2\alpha}$, respectively.

D. Ergodic capacity

The ergodic capacity of (3) is

$$C = \int_0^{+\infty} f_\gamma(\gamma) \log_2(1 + \gamma) d\gamma. \quad (28)$$

A closed form expression appears hard to obtain due to the complicated nature of (10); nevertheless, the integral can be evaluated numerically with Gauss-Laguerre quadrature. In [19], an approximation to (28) is given for $N = 1$. The following proposition provides upper and lower bounds to C for $N \geq 1$.

Proposition 2: The ergodic capacity of (3) is upper-bounded as

$$C < \bar{C} = \log_2 \left(1 + N\Gamma \left(\frac{1}{\alpha} + 1 \right) \left(\frac{M}{\lambda\delta} \right)^{1/\alpha} \right) \quad (29)$$

and lower bounded as

$$C \geq \underline{C} = \frac{1}{\alpha} \log_2 \left(\frac{M}{e^\Gamma \lambda \delta} \right) + \frac{H_{N-1}}{\ln 2}, \quad (30)$$

where $\Gamma = 0.577\dots$ is the Euler-Mascheroni constant and

$$H_n = \begin{cases} \sum_{k=1}^n \frac{1}{k} & n \geq 1 \\ 0 & n = 0 \end{cases} \quad (31)$$

is the n^{th} harmonic number. This bound is tight, i.e., $C \simeq \underline{C}$ for $\lambda \rightarrow 0$. A looser lower bound is

$$\underline{\underline{C}} = \frac{1}{\alpha} \log_2 \left(\frac{N^\alpha M}{e^\Gamma \lambda \delta} \right). \quad (32)$$

Proof: The upper bound is derived by noting that $E[\gamma] = E[a]E\left[\frac{1}{z}\right] = NE\left[\frac{1}{z}\right]$, so, for $N = 1$, $E\left[\frac{1}{z}\right] = E[\gamma]$. Setting $N = 1$ in (10), we have

$$E\left[\frac{1}{z}\right] = \frac{\lambda\delta\alpha}{M} \int_0^{+\infty} \gamma^\alpha e^{-c\gamma^\alpha} d\gamma = \left(\frac{M}{\lambda\delta} \right)^{1/\alpha} \Gamma \left(\frac{1}{\alpha} + 1 \right).$$

By applying Jensen's inequality⁹ on (28), we obtain (29).

For the derivation of the lower bound, from (15) and (28), we obtain

$$\begin{aligned} \underline{C} &= \frac{(-1)^N}{(N-1)! \ln 2} \int_0^{+\infty} \gamma^{N-1} \Phi_z^{(N)}(\gamma) \ln \gamma d\gamma \\ &= \frac{(-1)^N}{(N-1)! \ln 2} \sum_{k=0}^{N-2} (-1)^k \left[\Phi_z^{(N-k-1)}(\gamma) (\gamma^{N-1} \ln \gamma)^{(k)} \right]_0^{+\infty} \\ &\quad - \frac{1}{(N-1)! \ln 2} \int_0^{+\infty} \Phi'_z(\gamma) (\gamma^{N-1} \ln \gamma)^{(N-1)} d\gamma. \end{aligned} \quad (33)$$

⁹Jensen's inequality was also employed in [20] in order to derive an upper bound to the ergodic capacity, albeit in a slightly different context.

After some algebra, we can show that, for $k = 1, \dots, N - 1$, $N > 1$,

$$\begin{aligned} (\gamma^{N-1} \ln \gamma)^{(k)} &= (N-1) \dots (N-k) \gamma^{N-k-1} \ln \gamma \\ &+ \gamma^{N-k-1} \sum_{(l_1, \dots, l_{k-1})} (N-l_1) \dots (N-l_{k-1}) \end{aligned} \quad (34)$$

where the summation is taken over all permutations of the vector (l_1, \dots, l_{k-1}) , $l_j = 1, \dots, k$, $j = 1, \dots, k-1$. When $k = N - 1$, then

$$(\gamma^{N-1} \ln \gamma)^{(N-1)} = (N-1)! (\ln \gamma + H_{N-1}) \quad (35)$$

where H_n is defined in (31). From (16) and (34), we can show that the first term in (33) is zero.

Hence

$$\underline{C} = \frac{\lambda \delta \alpha}{M \ln 2} \int_0^{+\infty} \gamma^{\alpha-1} e^{-\frac{\lambda \delta}{M} \gamma^\alpha} \ln \gamma \, d\gamma + \frac{H_{N-1}}{\ln 2}$$

from which (30) follows by use of (4.331.1) on p.602 of [17].

Since the harmonic number is lower bounded as [21]

$$H_N > \ln N + \Gamma + \frac{1}{2(N+1)}$$

we have that

$$H_{N-1} = H_N - \frac{1}{N} > \ln N + \Gamma + \frac{1}{2(N+1)} - \frac{1}{N} > \log N, \quad N \geq 2.$$

The latter inequality holds because, for $N \geq 2$, $\frac{1}{N} - \frac{1}{2(N+1)} < \frac{1}{2} < \Gamma$, $\forall N \geq 2$. As a result, a looser lower bound to the capacity is (32). ■

Eq. (32) shows that \underline{C} is a linear function of $\log_2 \left(\frac{M}{\lambda \delta} \right)$, with slope $1/\alpha = b/2$ and a constant term $\log_2 N - \frac{\Gamma}{\alpha} \log_2 e$.

IV. NETWORK METRICS

Having evaluated the performance at the link level, we now turn our attention to network-wide metrics. Similarly to [1], we define the transmission capacity¹⁰ τ_ϵ as the maximum spatial

¹⁰In contrast to [1], where the SIR is constant across a packet, here the probability of packet error P_e is computed by averaging over different channel realizations. We can thus say that, on the average, the probability that a packet is received successfully is $1 - P_e$.

density of successful transmissions, multiplied by their rate $R_c M_c$, such that a constraint $P_e = \epsilon$ is satisfied, i.e.,

$$\tau_\epsilon = \lambda_\epsilon(1 - \epsilon)R_c M_c, \quad (36)$$

where λ_ϵ is the maximum contention density. A closed-form expression for λ_ϵ may be obtained by noting that, for $\epsilon \rightarrow 0$, we can take into account only Hamming distance error events in (9) and, moreover, $P_e \simeq \bar{P}_e$. The constraint that needs to be satisfied is therefore $\bar{P}_e \approx L_b w_L \bar{P}_L = \epsilon$. From Proposition 1, we find that

$$\lambda_\epsilon \approx \left(\frac{\epsilon}{K}\right)^{1/L} \frac{d_x^2 M}{16^\alpha \alpha B(N - \alpha, \alpha) \pi R^2} \quad (37)$$

where

$$K \triangleq \frac{L_b w_L}{2\pi} B(\alpha L + 1/2, \alpha L + 1/2) \quad (38)$$

is related to the code parameters and the propagation exponent. The maximum contention density of a coded system is therefore of the order $(\epsilon/L_b)^{1/L}$. This result is a manifestation of the channel diversity harnessed through frequency hopping and coding at the expense of spectrum. Moreover, note that λ_ϵ is proportional to $B(N - \alpha, \alpha)^{-1} \approx N^\alpha$, which is in agreement with the scaling law in [18].

The transmission capacity is upper-bounded by $\tau = \lambda C$, where C is the link ergodic capacity given by (28). From Proposition 2, a lower bound to τ is

$$\underline{\tau} = \frac{\lambda}{\alpha} \log_2 \left(\frac{N^\alpha M}{e^\Gamma \lambda \delta} \right). \quad (39)$$

Optimizing over λ , it is straightforward to verify that the optimal $\underline{\tau}$ is also proportional to N^α .

V. PHYSICAL-LAYER CONSIDERATIONS

This section discusses various physical-layer issues with respect to the system model presented in Section II. The influence of these on the decoder performance is assessed via simulation in Section VI.

A. Channel estimation

In this subsection, we discuss the important issue of how the decoder obtains estimates of \mathbf{h}_d and z_d in the d^{th} dwell. Assume that a header of T_p pilot symbols, selected from a complex PSK

constellation of zero mean and unit power, and known at the RX, is transmitted at the beginning of the dwell. If this header is denoted as \mathbf{p}_d^T , then, similarly to (1), the received pilot matrix is

$$\mathbf{Y}_d = \mathbf{h}_d \mathbf{p}_d^T + \mathbf{W}_d \quad (40)$$

where $\mathbf{W}_d = R^{b/2} \sum_{i \in \Pi} e_{d,i} r_i^{-b/2} e^{i\phi_i} \mathbf{h}_{d,i} \mathbf{p}_{d,i}^T$ and $[\mathbf{W}_d]_{n,t}$, $n = 1, \dots, N$, $t = 1, \dots, T_p$ are i.i.d. with $[\mathbf{W}_d]_{n,t} \sim \mathcal{CN}(0, z_d)$, given z_d .

An estimate of z_d can be obtained by

$$\hat{z} = \frac{1}{N(T_p - 1)} \left\| \left(\mathbf{I}_T - \frac{1}{T_p} \mathbf{p} \mathbf{p}^H \right) \mathbf{Y}^T \right\|^2, \quad (41)$$

where, for convenience, we have removed the subscript d . This estimate is obtained by finding jointly the maximum-likelihood (ML) estimators of \mathbf{h} and z (p.182, [22]), and multiplying the latter by the factor $T_p/(T_p - 1)$ in order to remove the bias. Intuitively, the estimate of the interference power is obtained by projecting the received signal onto the subspace which is orthogonal to the pilot data \mathbf{p} . Assuming that the estimate of z is accurate, i.e., $\hat{z} \approx z$, the minimum mean square error (MMSE) estimate of \mathbf{h} is ([22], p.391)

$$\hat{\mathbf{h}} = \frac{1}{z + T_p} \mathbf{Y} \mathbf{p}^* \quad (42)$$

and, defining $\boldsymbol{\epsilon} = \mathbf{h} - \hat{\mathbf{h}}$, it holds that $\hat{\mathbf{h}} \sim \mathcal{CN}\left(\mathbf{0}, \frac{T_p}{z + T_p} \mathbf{I}_N\right)$, $\boldsymbol{\epsilon} \sim \mathcal{CN}\left(\mathbf{0}, \frac{z}{z + T_p} \mathbf{I}_N\right)$ and $\hat{\mathbf{h}}, \boldsymbol{\epsilon}$ are independent. We can see that the estimate of \mathbf{h} is accurate if $T_p \gg z$.

Following the estimation of \mathbf{h} and z , the RX performs maximal ratio combining, i.e., it evaluates the product $\frac{\hat{\mathbf{h}}^H}{\|\hat{\mathbf{h}}\|^2} \mathbf{Y}$. From (1), we have

$$\frac{\hat{\mathbf{h}}^H}{\|\hat{\mathbf{h}}\|^2} \mathbf{Y} = \mathbf{x}^T + \frac{\hat{\mathbf{h}}^H}{\|\hat{\mathbf{h}}\|^2} (\boldsymbol{\epsilon} \mathbf{x}^T + \mathbf{W}). \quad (43)$$

Lumping the channel estimation error term with the interference, we can show that the equivalent channel model follows (3), with the SIR defined as

$$\gamma_{k,\text{csi}} = \frac{a_k}{z_k} \left(1 + \frac{1 + z_k}{T_p} \right)^{-1}. \quad (44)$$

The sequence $\{y_k, \gamma_{k,\text{csi}}\}_{k=1}^{DT_d}$ is the input to decoder (6).

A consequence of channel estimation is the loss of information rate by a factor $\frac{T_d}{T_d + T_p}$, due to the transmission of the pilot symbols in each dwell. This factor must be taken into account when evaluating the transmission capacity.

B. Correlation of the interference

Eq. (8) is based on the assumption that the coded bits encounter independent SIR conditions across the span of an error event in the decoder. The assumption is justified if, (a) there is a sufficient number of dwells¹¹ such that, due to interleaving, these bits will be transmitted on different dwells, and (b) the SIRs are independent across dwells. Given that the coherence bandwidth of the channel is equal to the width of a subband, the latter assumption is reasonable if the number of frequencies is sufficiently large. As shown in [23], the temporal correlation of the interference in a fixed Poisson network of transmitters and Rayleigh fading is $p/2$, where p is the random access probability. In this paper, random access is achieved via random frequency hopping, i.e., p can be substituted by $1/M$.

C. Synchronization

The assumption of synchronization of different TX-RX pairs in the network at the dwell level results in a worst-case scenario in terms of the interference power level. On the other hand, it also results in a best-case scenario in terms of the correspondence of the estimated interference level to that encountered in the remainder of the dwell. In this respect, asynchronous transmissions may require the insertion of more pilot symbols throughout the dwell and, consequently, the loss of rate. The mismatch between the actual and estimated interference power will incur a performance loss, the study of which is beyond the scope of the present paper.

D. Power control

In [2], it was shown that channel inversion PC increases the outage probability in a random ad hoc network with fading. In order to examine the effect of PC in the context of this paper, we assume that the typical TX-RX link is subject to lognormal shadowing, i.e., the transmitted signal is multiplied by a r.v. $S = 10^{\sigma_s \xi / 10}$, where $\xi \sim \mathcal{N}(0, 1)$ and, typically, $\sigma_s = 6 - 8$ dB. Note that S (like the node locations) is assumed to be a “long-term” random variable, i.e., it is constant for at least the duration of a packet slot.

In order to take shadowing into account in the analysis of Section III, the definition of the constant δ in (5) for the case of channel inversion PC must be modified as $\delta_{\text{pc}} = \pi\Gamma(1 -$

¹¹This is also related to the length of the codeword.

$\alpha)R^2\mathbb{E}[(S^\alpha S'^{-\alpha}]$, where S models the shadowing between TX_i and RX_0 and S' models the shadowing between TX_i and its corresponding RX . In the absence of PC, we have $\delta_{\text{npc}} = \pi\Gamma(1-\alpha)R^2\mathbb{E}[S^\alpha]S'^{-\alpha}$, where S' now denotes the shadowing between TX_0 and RX_0 . Therefore, in the case of no PC, P_l in (8) is conditioned on the realization of S' and the expectation of the former with respect to the latter must be taken in order to obtain the unconditional probability of codeword/packet error.

VI. NUMERICAL RESULTS

In this section, we present numerical results for a network with default parameters $R = 1$ m, $M = 100$, $M_c = 2$ (4QAM), $N = 2$ and $b = 4$. Six rate $R_c = 1/2$ convolutional codes are considered, with memory, minimum Hamming distances and distance spectra listed in Table II (see [24] for more details). In all plots, the upper bound to the pairwise error probability \bar{P}_l is evaluated by (22). We also define the parameter $N_{\text{eff}} = \frac{\lambda\pi R^2}{M}$, i.e., the expected number of TXs in the transmission range per subband, as a measure of the interference level in the network.

In the simulations, we generate a new network realization for every transmitted packet. At the TX, we employ a block interleaver of vertical dimension equal to the number of bits per dwell $M_c T_d$ and horizontal dimension equal to D , such that $M_c T_d$ consecutive codeword bits are guaranteed to be transmitted on different dwells. The coherence time of the fading is taken to be equal to the duration of a packet. In this manner, we can compare the MA scheme proposed in this paper with the slow FH (IA) scheme advocated in [12].

In Fig. 1, we plot the FEP vs. N_{eff}^{-1} for the codes listed in Table II and $L_b = 800$. The upper bound (9) is plotted with a solid line, when error events up to length $L + 4$ are taken into account, and with a dotted line, when only the Hamming distance error events are taken into account. As expected, for each code, the two curves converge as $N_{\text{eff}} \rightarrow 0$. We also simulate the performance of the codes by dividing the packet in $D = 40$ dwells of $T_d = 20$ 4QAM symbols. Fig. 1 demonstrates that the dotted curve is quite accurate for $P_e < 0.01$ and Enc1-Enc5, however it is slightly optimistic in the case of Enc6. This is attributed to the impact of channel correlation within the packet the effect of which becomes more apparent as the decoder Hamming distance (hence the span of the error events) becomes larger.

In Fig. 2, we plot the simulated FEP vs. N_{eff}^{-1} , for Enc4 and decreasing values of the number of subbands M . As M decreases the diversity order decreases, as the probability that the same

fading condition and/or the same interferer are encountered across dwells increases (and the assumption of independent channel conditions thus becomes obsolete). The simulated P_e in the case of slow FH is also shown for comparison; note that even for $M = 4$, the gain of the scheme considered in this paper compared to slow FH is still considerable, as the diversity order of the latter is only one.

In Fig. 3, we plot the maximum contention density λ_ϵ , evaluated by (37), vs. L , for the set of parameters of Fig. 1 and different values of the ratio ϵ/w_L . Note that, for $\epsilon/w_L = 0.001$, increasing the diversity order of the code from 3 to 8, results in a tenfold increase of λ_ϵ . The gain comes at an increase of the decoder memory from 1 to 5.

Fig. 4 presents the results of Proposition 2 on the link ergodic capacity for two different values of N . As expected, (29) and (30) become tight as $N_{\text{eff}} \rightarrow \infty$ and $N_{\text{eff}} \rightarrow 0$, respectively.

In Fig. 5, we employ the channel estimation scheme of Section V and examine the effect of imperfect CSI via simulation, when $L_b = 500$, $D = 25$ and $T_d = 20$. For $T_p = 5$ and a rate-loss factor of 20% there is a 1 dB penalty compared to the perfect-CSI case. As T_p is increased the performance loss is reduced, at the expense of information rate, e.g., at $T_p = 10$, the rate-loss factor is 2/3.

Finally, in Fig. 6, the simulated FEP is plotted vs. N_{eff}^{-1} for Enc2 and Enc4, for a channel with lognormal shadowing ($\sigma_s = 6$ dB) and shadowing-inversion PC or no PC. For small N_{eff} , PC introduces a substantial gain, e.g., for Enc4 at $N_{\text{eff}} = 10$ dB, this gain is an order of magnitude. The reason for this is that the detrimental effect of shadowing to RX_0 is canceled and, at the same time, the interferer process is sparse enough such that the code protects RX_0 in the unlikely event of a large interfering power from a nearby interferer¹². Theoretically, we can see this with the help of Jensen's inequality; given that all shadowing variables are i.i.d., by the definitions of δ_{pc}^l and δ_{npc}^l in Section V-D, we have that $\delta_{\text{pc}}^l = \text{E}[S^\alpha]^l \text{E}[S^\alpha]^l < \text{E}[S^{\alpha l}] \text{E}[S^\alpha]^l = \delta_{\text{npc}}^l$. Hence, from Proposition 1, PC should perform better in the small FEP regime, which is verified by Fig. 6. On the other hand, as the network becomes very dense, the diversity in the received signal is lost and the decoder is overwhelmed by an increased interference level due to PC. This is more apparent for Enc2 than Enc4, since Enc2 has a smaller Hamming distance. On a final note, in the case of PC, we observe that there is good agreement between (9) and the simulation

¹²This occurs when deep shadowing afflicts the channel between that interferer and its respective RX.

results.

VII. CONCLUDING REMARKS

In this paper we considered FH during packet transmission and coding, as a physical layer scheme for random wireless networks with uncoordinated transmissions. We demonstrated via analysis and simulation that the transmission capacity scales as $\epsilon^{1/L}$, where ϵ is the constraint placed on the packet error probability and L is the code diversity order. A byproduct of our analysis was the derivation of a compact expression for the pdf of the SIR in a Rayleigh fading and α -stable interference channel, when the RX performs MRC. Upper and lower bounds on the ergodic capacity of this channel were also derived.

Employing a simple channel estimation algorithm based on the transmission of pilot symbols at the beginning of each dwell, we showed that the performance degradation due to imperfect CSI is reasonable, at a rate loss of the order of 20%. The effect of channel inversion PC was also confirmed for a channel with lognormal shadowing and PC was shown to be beneficial if λ/M is sufficiently small. In conclusion, we believe that, given the gains in terms of network capacity at moderate encoding/decoding complexity, even for a small number of subbands, this scheme merits consideration despite the increased overhead compared to a slow FH system.

REFERENCES

- [1] S. P. Weber, X. Yang, J. G. Andrews, and G. de Veciana, "Transmission capacity of wireless ad hoc networks with outage constraints," *IEEE Trans. Inf. Theory*, vol. 51, pp. 4091–4102, Dec. 2005.
- [2] S. P. Weber, J. G. Andrews, and N. Jindal, "The effect of fading, channel inversion and threshold scheduling on ad hoc networks," *IEEE Trans. Inf. Theory*, vol. 53, pp. 4127–4149, Nov. 2007.
- [3] M. Haenggi, J. G. Andrews, F. Baccelli, O. Dousse, and M. Franceschetti, "Stochastic geometry and random graphs for the analysis and design of wireless networks," September 2009, *to appear in the IEEE Journal on Selected Areas in Communications*.
- [4] D. N. C. Tse and P. Viswanath, *Fundamentals of Wireless Communication*, 1st ed. Cambridge University Press, 2005.
- [5] K. Stamatiou, J. G. Proakis, and J. R. Zeidler, "Evaluation of MIMO techniques in FH-MA ad hoc networks," in *Proc. IEEE GLOBECOM*, Washington D.C., Nov. 2007.
- [6] G. Caire, G. Taricco, and E. Biglieri, "Bit-interleaved coded modulation," *IEEE Trans. Inf. Theory*, vol. 44, pp. 927–946, May 1998.
- [7] E. Geraniotis and J. W. Gluck, "Coded FH/SS communications in the presence of combined partial-band noise jamming, rician nonselective fading and multiuser interference," *IEEE J. Sel. Areas Commun.*, vol. 5, pp. 194–214, Feb. 1987.
- [8] C. W. Baum and M. B. Pursley, "Erasure intertion in FH communications with fading and partial-band interference," *IEEE Trans. Veh. Technol.*, vol. 46, pp. 949–956, Nov. 1997.

- [9] J. G. Proakis and M. Salehi, *Digital Communications*, 5th ed. Mc Graw Hill, 2008.
- [10] M. W. Subbarao and B. L. Hughes, "Optimal transmission ranges and code rates for frequency-hop packet radio networks," *IEEE Trans. Commun.*, vol. 4, pp. 670–678, Apr. 2000.
- [11] H. Sui and J. R. Zeidler, "Information efficiency and transmission range optimization for coded MIMO FH-CDMA networks in time-varying environments," *IEEE Trans. Commun.*, vol. 57, pp. 481–491, Feb. 2009.
- [12] J. G. Andrews, S. Weber, and M. Haenggi, "Ad hoc networks: to spread or not to spread?" *IEEE Commun. Mag.*, pp. 84–91, Dec. 2007.
- [13] G. Caire and E. Viterbo, "Upper bound on the frame error probability of terminated trellis codes," *IEEE Commun. Lett.*, vol. 2, pp. 2–4, Jan. 1998.
- [14] E. S. Sousa and J. A. Silvester, "Optimum transmission ranges in a direct-sequence spread-spectrum multi-hop packet radio network," *IEEE J. Sel. Areas Commun.*, vol. 8, pp. 762–771, Jun. 1990.
- [15] F. Baccelli, B. Błaszczyszyn, and P. Mühlethaler, "An Aloha protocol for multi-hop mobile wireless networks," *IEEE Trans. Inf. Theory*, vol. 52, pp. 421–436, Feb. 2006.
- [16] M. K. Simon and D. Divsalar, "Some new twists to problems involving the Gaussian probability integral," *IEEE Trans. Commun.*, vol. 46, pp. 200–210, Feb. 1998.
- [17] I. S. Gradshteyn and I. M. Ryzhik, *Table of integrals, series and products*, 4th ed. Academic Press, 1994.
- [18] A. M. Hunter, J. G. Andrews, and S. P. Weber, "Capacity scaling of ad hoc networks with spatial diversity," *IEEE Trans. Wireless Commun.*, vol. 7, pp. 5058–5071, Dec. 2008.
- [19] M. Haenggi, "Outage and local throughput and capacity of random wireless networks," 2009, *submitted for publication in the IEEE Trans. on Wireless Commun.*
- [20] D. W. B. S. Govindasamy and D. H. Staelin, "Spectral efficiency in single-hop ad hoc wireless networks with interference using adaptive antenna arrays," vol. 25, pp. 1358–1369, Sep. 2007.
- [21] R. M. Young, "Euler's constant," *The Mathematical Gazette*, vol. 75, pp. 187–190, 1991.
- [22] S. M. Kay, *Fundamentals of statistical signal processing: estimation theory*, 1st ed. Prentice Hall, 1993.
- [23] R. K. Ganti and M. Haenggi, "Spatial and temporal correlation of the interference in ALOHA ad hoc networks," 2009, *submitted to the IEEE Comm. Letters, available at <http://arxiv.org/abs/0904.1444>.*
- [24] M. L. Cedervall and R. Johannesson, "A fast algorithm for computing distance spectrum of convolutional codes," *IEEE Trans. Inf. Theory*, vol. 35, pp. 1146–1159, Nov. 1989.

TABLE I: Commonly used symbols

Symbol	Meaning
R	Distance of typical TX-RX link
λ	Density of TXs
M	Number of subbands
N	Number of RX antennas
b	Path-loss exponent ($b > 2$)
$\alpha = 2/b$	Stability exponent
L_b	Number of information bits per packet
M_c	Number of bits per constellation symbol
R_c	Rate of convolutional code
T_d	Number of data symbols per dwell
T_p	Number of pilot symbols per dwell
D	Number of dwells
L	Hamming distance of convolutional code
P_l	Probability of length- l error event
w_l	Number of length- l error events
P_e	Probability of packet error
C	Ergodic capacity of typical TX-RX link
τ_ϵ	Transmission capacity under constraint $P_e = \epsilon$

TABLE II: Optimum rate 1/2 convolutional codes

Encoder	Memory	L	w_L, \dots, w_{L+4}
Enc1	1	3	1,1,1,1,1
Enc2	2	4	2,0,5,0,13
Enc3	3	5	1,0,6,0,16
Enc4	3	6	1,3,5,11,25
Enc5	5	8	2,7,10,18,49
Enc6	7	10	1,6,13,20,64

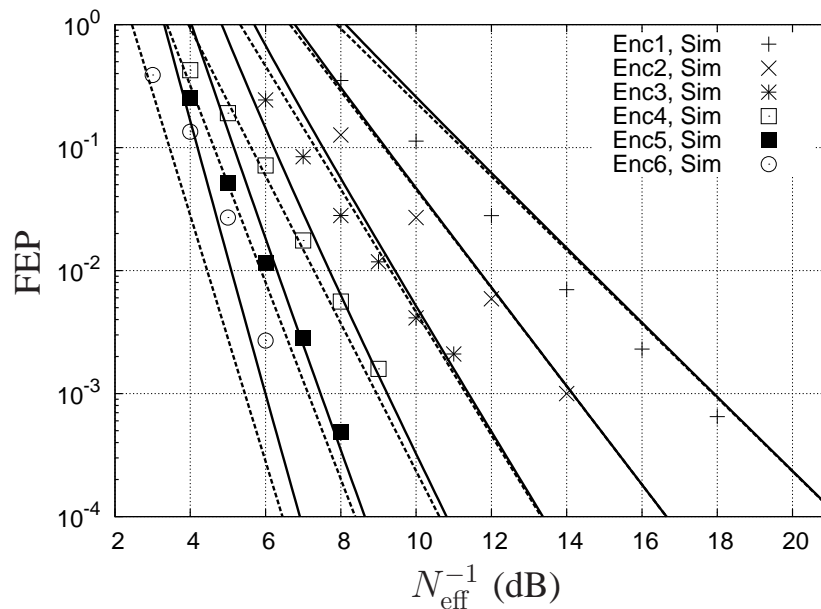


Fig. 1: FEP vs. N_{eff}^{-1} for the codes in Table II. The solid (dotted) lines depict (9) with error events up to length $L + 4$ (L) taken into account (4QAM, $L_b = 800$, $D = 40$, $T_d = 20$, $N = 2$, $b = 4$, perfect CSI).

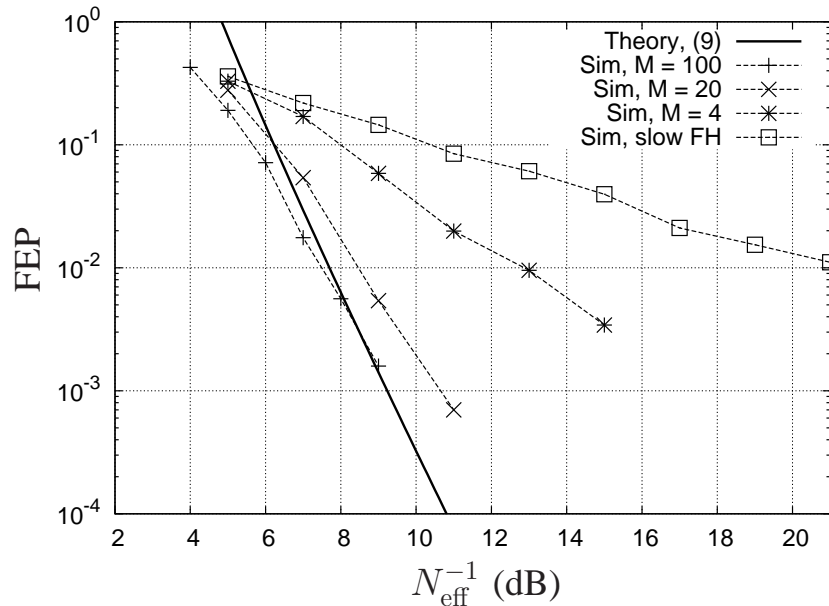


Fig. 2: FEP vs. N_{eff}^{-1} for Enc4 and $M = 4, 20, 100$. The simulated performance for slow FH is also shown for comparison. (4QAM, $L_b = 800$, $D = 40$, $T_d = 20$, $N = 2$, $b = 4$, perfect CSI).

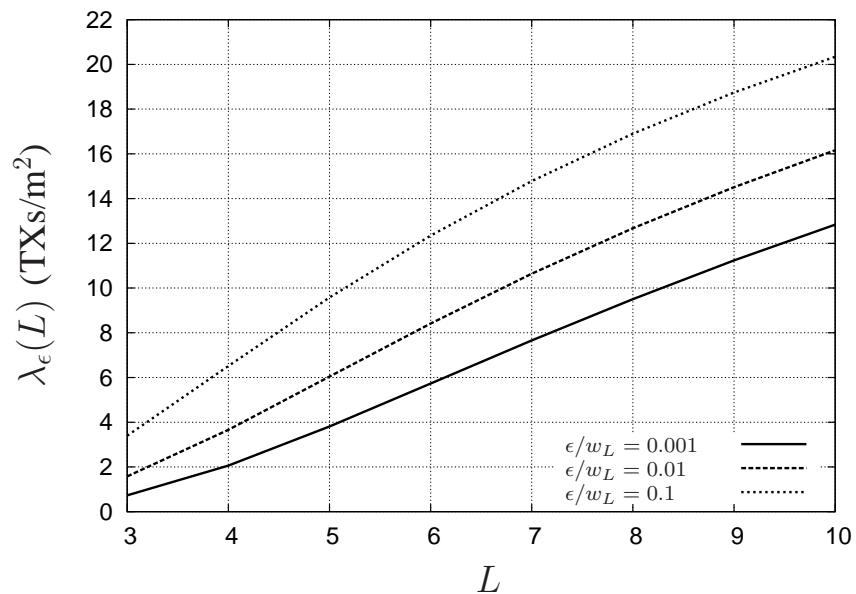


Fig. 3: Maximum contention density vs. L for different values of ϵ/w_L ($R = 1$ m, 4QAM, $L_b = 800$, $N = 2$, $b = 4$, perfect CSI).

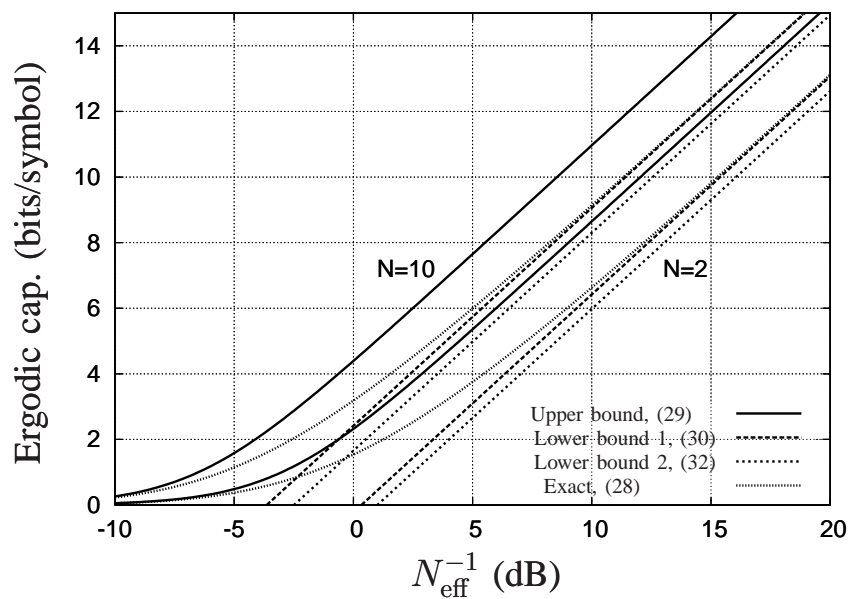


Fig. 4: Link ergodic capacity vs. N_{eff}^{-1} . The two groups of curves correspond to $N = 2, 10$ ($b = 4$).

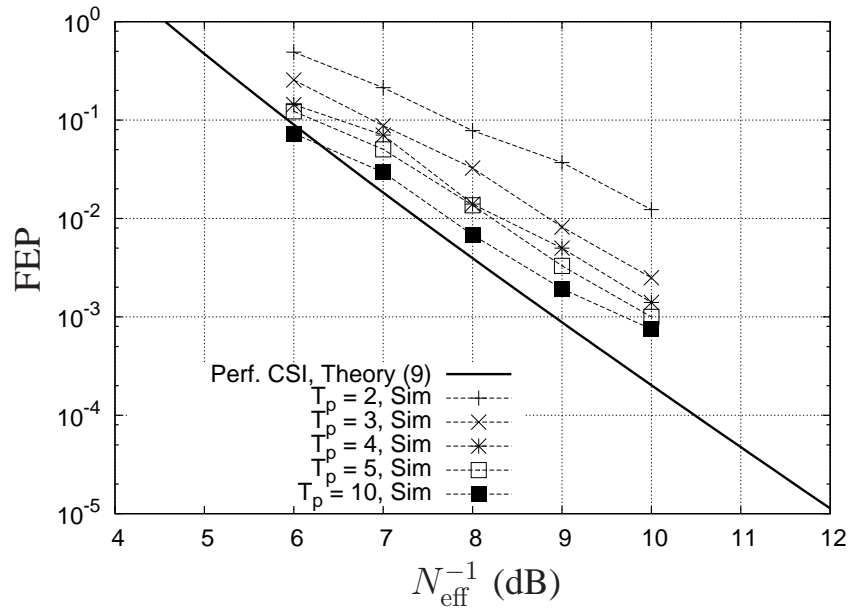


Fig. 5: FEP vs. N_{eff}^{-1} for Enc1 and different values of T_p (4QAM, $L_b = 500$, $D = 25$, $T_d = 20$, $N = 2$, $b = 4$).

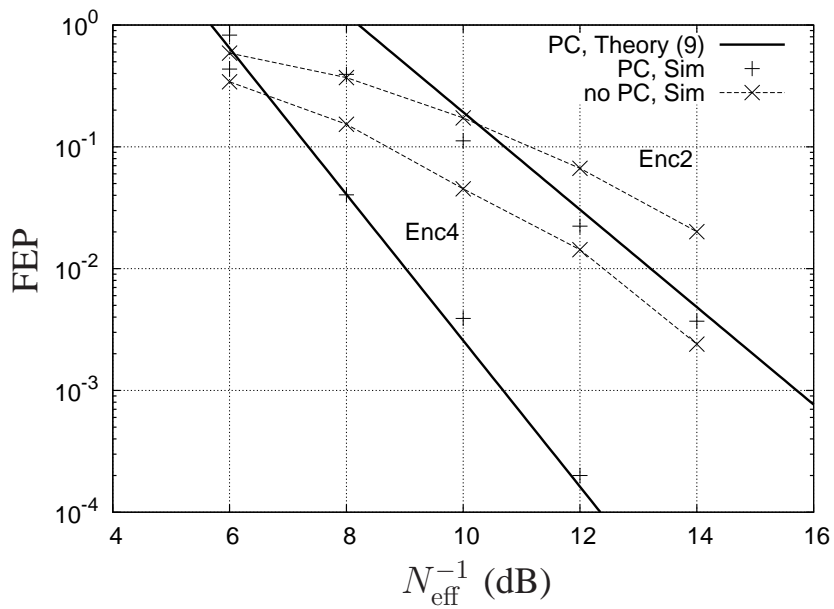


Fig. 6: FEP vs. N_{eff}^{-1} for Enc2 and Enc4 with/without PC (4QAM, $L_b = 500$, $D = 25$, $T_d = 20$, $N = 2$, $b = 4$, perfect CSI, $\sigma_s = 6$).